Variable Stiffness Actuators: A Port-Based Power-Flow Analysis

Raffaella Carloni, *Member, IEEE*, Ludo C. Visser, *Student Member, IEEE*, and Stefano Stramigioli, *Senior Member, IEEE*

***Abstract*—Variable stiffness actuators realize a novel class of actuators, which are capable of changing the apparent output stiffness independently of the output position. This is mechanically achieved by the internal introduction of a number of elastic elements and a number of actuated degrees of freedom (DOFs), which determine how the elastic elements are sensed at the output. During the nominal behavior of these actuators, the power flow from the internal actuated DOFs can be such that energy is undesirably stored in the elastic elements because of the specific kinematic structure of the actuator. In this study, we focus on the analysis of the power flow in variable stiffness actuators. More specifically, the analysis is restricted to the kinematic structure of the actuators, in order to show the influence of the topological structure on the power flow, rather than on the realization choices. We define a measure that indicates the ratio between the total amount of power that is injected by the internal actuated DOFs and the power that is captured by the internal elastic elements which, therefore, cannot be used to do work on the load. In order to define the power-flow ratio, we exploit a generic port-based model of variable stiffness actuators, which highlights the kinematic properties of the design and the power flows in the actuator structure.**

***Index Terms*—Dynamics, kinematics, port-based modeling, variable stiffness actuators.**

I. Introduction

In applications in which robots need to interact with the environment or humans, if the actuation is too stiff, instability can occur during the interaction, leading to possible damage to the robot or even injuries to humans. The instability can be effectively dealt with by using impedance control strategies [1]. However, since the reliability of this approach depends on software implementation, a mechanical compliance can be added in the robot actuation to ensure intrinsic safe interaction. By making this compliance variable, and thus realizing *variable stiffness actuators*, the apparent stiffness of the robot can be tuned to a specific task, and it is possible to achieve the tradeoff between precision of motion and robustness [2], [3]. Given the broad range of possible applications of variable stiffness actuators, the research effort to design such actuators is increasing.

Manuscript received April 21, 2011; revised August 26, 2011; accepted September 8, 2011. Date of publication October 7, 2011; date of current version February 9, 2012. This paper was recommended for publication by Associate Editor E. Guglielmelli and Editor B. J. Nelson upon evaluation of the reviewers' comments. This work was supported by the European Commission's 17th Framework Program as part of the Project Variable Impedance ACTuation systems embodying advanced interaction behaviORS (VIACTORS) under Grant 231554.

The authors are with the Department of Electrical Engineering, Faculty of Electrical Engineering, Mathematics and Computer Science, University of Twente, Enschede 7500 AE, The Netherlands (e-mail: r.carloni@utwente.nl; l.c.visser@utwente.nl; s.stramigioli@utwente.nl).

Digital Object Identifier 10.1109/TRO.2011.2168709

Many different designs have been presented, based on different working principles [4]. For example, "Jack Spring" varies the number of active coils of an internal spring [5], and the actuator presented in [6] changes the configuration of permanent magnets to achieve a variable stiffness. However, most variable stiffness actuator designs internally present a set of elastic elements, usually springs, and a set of actuated degrees of freedom (DOFs). The mechanics is such that the apparent output stiffness is determined by the intrinsic properties of the elastic elements and by the configuration of the internal DOFs. For example, in VSA [7], VSA-II [8], and VS-Joint [9], the change of the stiffness is realized by changing the pretension of the internal nonlinear springs. In other actuators, including vsaUT [10], [11], AwAS [12], AwAS-II [13], and HDAU [14], the change of the apparent output stiffness is obtained by changing the transmission ratio between the internal linear springs and the actuator output by implementing a lever arm with a variable effective length.

By the comparison of different working principles, and therefore, different kinematic structures, it can be observed that, during a dynamic behavior of the actuators, part of the power flow from the internal DOFs is directed to the internal elastic elements, instead of to the load. This implies that potential energy is undesirably stored in the elastic elements.

In this paper, we evaluate the power flow in variable stiffness actuators with main focus on the amount of energy that is captured by the internal elastic elements during a nominal functioning of the actuator. In particular, the aim of this study is to analyze the influence of the actuator kinematics on the power flow in the system. This allows an evaluation of the topology of the actuator without the consideration of the internal friction or dissipation, which are due to specific realization choices. In an earlier study, we already defined a measure of energy consumption during the change of the apparent stiffness [15]. We showed that, under static conditions, the amount of energy that is used by a variable stiffness actuator to change the apparent output stiffness is strongly influenced by its kinematic properties.

We define a power-flow ratio under dynamic conditions that measures how much power can be transferred from the internal DOFs to the output, because of the actuator kinematic design, irrespective of the dynamic behavior of the load. We show that, for different principle designs, this power-flow ratio is strictly related to the kinematic properties of the actuator, and it is independent of the task that is realized by the load. The power-flow ratio is derived from the analysis of a port-based model of variable stiffness actuators, which is introduced in [10] and [11],

that highlights the power flows inside the actuator structure and of the actuator toward the external environment.

The paper is organized as follows. In Section II, we describe a port-based framework of variable stiffness actuators, which provides the necessary background for the power-flow analysis and the derivation of the power-flow ratio. In Section III, a port-based model of variable stiffness actuators is presented, with particular attention to the analysis of the actuator kinematics. In Section IV, we present a power-flow analysis, which highlights how the power from the control port is distributed between the internal elastic elements and the output port, and we define the power-flow ratio, which is, then, computed for some variable stiffness actuator design principles in Section V. Concluding remarks are given in Section VI.

II. Port-Based Modeling Framework

In this section, we briefly describe the port-based modeling framework and the bond-graph representation. Further reading can be found in [16] and [17].

A. Port-Based Modeling

The fundamental concept behind the port-based modeling framework is that any physical system can be seen as the interconnection of simple elements, which are characterized by a specific energetic behavior. The interconnections are realized by ports, which are defined by a pair of power conjugate variables, namely flows and efforts. For example, in the mechanical domain, the flows are interpreted as velocities and the efforts as forces.

Let f be an element of the linear space of flows $\mathcal{F}$, and e be an element of the dual linear space of efforts[1] $\mathcal{E} := \mathcal{F}^*$. The dual product $\langle e|f\rangle$ yields power, and therefore, a pair of conjugate variables defines a power flow P on the total space of port variables, i.e.,

$$P = \langle e|f\rangle, \quad (f,e) \in \mathcal{F} \times \mathcal{E}.$$

The distribution of power flow among the different ports of the physical system is described by a power continuous network topology. A *Dirac structure* on $\mathcal{F} \times \mathcal{E}$ is a subspace $\mathcal{D} \subset \mathcal{F} \times \mathcal{E}$, with $\dim\mathcal{D} = \dim\mathcal{F}$, such that

$$\langle e|f\rangle = 0 \quad \forall\,(f,e) \in \mathcal{D}. \tag{1}$$

This relation defines power conservation, and therefore, it implies that the total power entering, or leaving, a Dirac structure is zero. The behavior of any physical system can be modeled by making its network topology explicit, i.e., its Dirac structure.

The generic network topology is shown in Fig. 1, where the following four separate power ports can be distinguished.

1) The *storage port* interconnects the internal energy storage elements $\mathbb{C}$, which represents storage of either generalized potential or generalized kinetic energy. If H is the Hamiltonian energy function of the system, the power conjugate variables (f_S, e_S) at this port satisfy the energy balance
$$\frac{dH}{dt} = \langle e_S|f_S\rangle. \tag{2}$$
2) The *dissipative port* interconnects the energy dissipation element $\mathbb{R}$ and is characterized by the power conjugate variables (f_R, e_R).
3) The *control port*, which is characterized by the power conjugate variables (f_C, e_C), is used for the control actions.
4) The *interaction port*, which is characterized by the power conjugate variables (f_I, e_I), represents the interactions with the environment, i.e., (a composition of) other physical systems.

[1]Under coordinate transformations, efforts behave as covectors. However, for notational convenience, we denote them as vectors in this study.

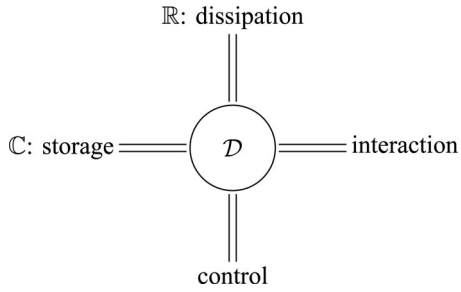

Fig. 1. Generic network structure of a physical system. The Dirac structure $\mathcal{D}$ defines a power continuous interconnection between the ports. Internal energy storage is represented by a $\mathbb{C}$-element and energy dissipation by the $\mathbb{R}$-element. The system interacts with the environment via the control and interaction ports.

Since, from the definition in (1), the Dirac structure $\mathcal{D}$ is a power continuous network topology, it follows that

$$\langle e_S|f_S\rangle + \langle e_R|f_R\rangle + \langle e_I|f_I\rangle + \langle e_C|f_C\rangle = 0 \tag{3}$$

and by the substitution of (2)

$$\frac{dH}{dt} = -\langle e_R|f_R\rangle - \langle e_I|f_I\rangle - \langle e_C|f_C\rangle$$

i.e., the rate of change of the internal energy is determined by the amount of dissipated energy, and the power flow through the interaction and the control ports. This means that the system is passive with respect to these input ports.

A Dirac structure can describe any power continuous network topology, which can be either constant or configuration dependent. Therefore, it provides a complete way to describe any physical system dynamics. In particular, it highlights the power flows inside the system itself and of the system toward the external environment. With respect to variable stiffness actuators, by describing each actuator in terms of its Dirac structure, it is possible to identify both common components and different dynamic behaviors among the various designs. This means that, by deriving, for each actuator, the corresponding Dirac structure, the different actuators kinematics can be thoroughly analyzed and compared.

B. Bond-Graph Representation

The concept of network topologies, and thus of Dirac structures, allows a compact graphical representation. By the use of bond graphs, we can represent the generic physical system of Fig. 1 as in Fig. 2, where the half-arrows are *multibonds*

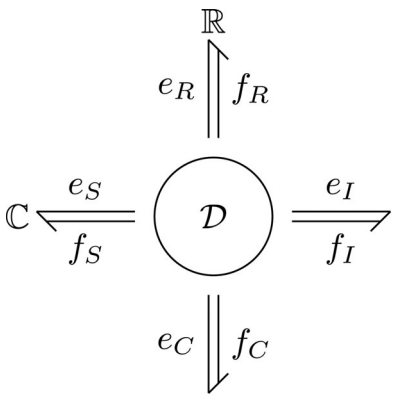

Fig. 2. Bond-graph representation of a generic physical system. $\mathcal{D}$ represents the Dirac structure; $\mathbb{C}$ represents the energy-storage element; and $\mathbb{R}$ represents the energy-dissipation element.

and denote the multidimensional interconnections between the different parts of the system. Note that the power flow $\langle e|f\rangle$ is defined positive in the direction of the half-arrow, and, in order to comply with the power continuity constraint (1), all bonds must have the same orientation with respect to the Dirac structure.

Throughout the paper, some fundamental interconnection elements are used to detail the Dirac structure that models the variable stiffness actuators. Essentially, these elements are examples of Dirac structures, and since a composition of Dirac structures is again a Dirac structure, these basic elements can give more insights when modeling the behavior of a complex system. Specifically, these are as follows.

1) A 1-*junction* defines a common flow interconnection, e.g., a rigid connection between two masses such as the actuator output port and a load. In order to satisfy (1), the behavior of a 1-junction, with N connected bonds, satisfies

$$f_1 = \cdots = f_N, \quad \sum_{i=1}^{N} e_i = 0. \tag{4}$$

2) The dual of a 1-junction is a 0-*junction*, which defines a common effort interconnection. The behavior of a 0-junction, for N connected bonds, is given by

$$\sum_{i=1}^{N} f_i = 0, \quad e_1 = \cdots = e_N. \tag{5}$$

3) A modulated transformer ($\mathbb{MTF}$)-element defines a power continuous transformation between two ports. An example is an ideal gearbox: If the input and the output of the gearbox are characterized by power conjugate variables $(f_{\text{in}}, e_{\text{in}})$ and $(f_{\text{out}}, e_{\text{out}})$ and α is the transformation ratio (either a scalar or a matrix), the behavior for the two ports is described as

$$f_{\text{out}} = \alpha\, f_{\text{in}}, \quad e_{\text{in}} = \alpha^T\, e_{\text{out}}.$$

It is readily verified that any combination of these elements again yields a power continuous interconnection structure.

III. Port-Based Model of Variable Stiffness Actuators

In this section, we describe a generic port-based model of variable stiffness actuators. This is possible by identifying common components of the actuators and describing the interconnection among these components by means of a generic Dirac structure. For any actuator, a specific representation of the Dirac structure can be found by explicitly describing the kinematics of its design. Dynamic properties of different designs can then be derived by analyzing the respective Dirac structures. The generic port-based model has been introduced in [10] and [11], and here, we intend to revisit the aspects that are relevant for the remainder of this paper.

A. Variable Stiffness Actuators as Dirac Structures

For the derivation of a generic model for variable stiffness actuators, we made the following assumptions.

1) The actuator output is 1-D and is characterized by the generalized configuration variable $r \in \mathcal{R}$.
2) The actuator has a number n_s of internal elastic elements, e.g., springs, which can be either linear or nonlinear. The elastic elements are characterized by the state, i.e., $s \in \mathcal{S}$, and by the positive-semidefinite energy function, i.e., $H(s) : \mathcal{S} \to \mathbb{R}$, that describes the amount of stored elastic energy.
3) Internally, there are $n_q \geq n_s$ actuated DOFs, which are characterized by the generalized configuration variables $q \in \mathcal{Q}$. These DOFs determine how the elastic elements are sensed at the output, and in particular, they determine the apparent output stiffness K of the actuator, which is locally defined as

$$K := \frac{\delta F}{\delta r}$$

i.e., the ratio of the infinitesimal change of the actuator-generalized output force δF as a result of an infinitesimal displacement of the actuator output position δr.

Moreover, in our model, we ignore internal friction and inertias, since we focus on the working principles and the kinematics of the actuator design, rather than on the details of the implementation.

By these assumptions, we identify the common components of the different variable stiffness actuator designs, i.e., the elastic elements, the internal DOFs, and the interaction port. From the analysis of the kinematics, we derive how the different components are interconnected and how the power flows among them.

The generic model of a variable stiffness actuator is depicted, by means of bond graphs, in Fig. 3. The $\mathbb{C}$-element represents the storage of elastic energy by the internal elastic elements. The power conjugate variables (f_S, e_S) are

$$\dot{s} = f_S, \quad e_S = \frac{\partial H}{\partial s}(s).$$

The control port is characterized by the power conjugate variables (f_C, e_C), which correspond to $(\dot{q}, \tau)$, i.e., the rate of

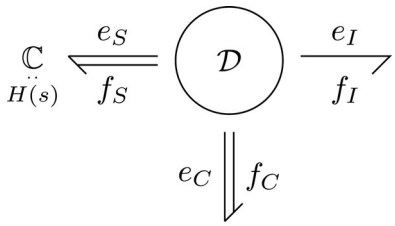

Fig. 3. Port-based representation of variable stiffness actuators. The $\mathcal{D}$-element represents the Dirac structure. The internal elastic elements are represented by the multidimensional $\mathbb{C}$-element, with state s and elastic energy function $H(s)$. The internal DOFs are actuated via the control port (f_C, e_C), while the interconnection with the load is via the output port (f_I, e_I).

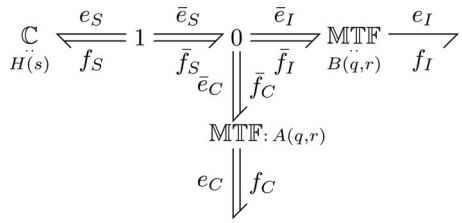

Fig. 4. Variable stiffness actuators. The Dirac structure expressed in (6) can be detailed by using two $\mathbb{MTF}$-elements, which implement the maps that are defined by $A(q,r)$ and $B(q,r)$. The 1- and 0-junctions implement power continuous connections, with common flow and common effort, respectively.

change of the configuration variables q of the internal DOFs and the collocated generalized forces τ, respectively. The interaction port is characterized by the power conjugate variables (f_I, e_I), which correspond to $(\dot{r}, F)$, i.e., the rate of change of the actuator output position r and the generalized output force F. The Dirac structure $\mathcal{D}(q,r)$ defines the interconnection, and it is explicitly allowed to depend on the configuration variables q and r. The requirement of power continuity imposes a constraint relation between the power conjugate variables, which can be expressed in a matrix form as

$$\begin{bmatrix} f_S \\ e_C \\ e_I \end{bmatrix} = \underbrace{\begin{bmatrix} 0 & A(q,r) & B(q,r) \\ -A^T(q,r) & 0 & 0 \\ -B^T(q,r) & 0 & 0 \end{bmatrix}}_{D(q,r)} \begin{bmatrix} e_S \\ f_C \\ f_I \end{bmatrix} \tag{6}$$

in which the matrix $D(q,r)$ represents the Dirac structure. The skew-symmetry of $D(q,r)$ establishes the power continuity of the interconnection, as stated in (1).

The Dirac structure of Fig. 3 is made explicit in Fig. 4. The $\mathbb{MTF}$-elements implement the maps $A(q,r)$ and $B(q,r)$, such that

$$\bar{f}_C = A(q,r)\, f_C, \quad e_C = A^T(q,r)\, \bar{e}_C$$
$$\bar{f}_I = B(q,r)\, f_I, \quad e_I = B^T(q,r)\, \bar{e}_I$$

where the port variables $(\bar{f}_C, \bar{e}_C)$, $(\bar{f}_I, \bar{e}_I)$, and $(\bar{f}_S, \bar{e}_S)$ are introduced on the corresponding bonds. The 0-junction represents a power continuous common effort connection, which is defined in (5), such that

$$\bar{f}_S = \bar{f}_I + \bar{f}_C, \quad \bar{e}_S = \bar{e}_I = \bar{e}_C.$$

The Dirac structure representation is completed with the 1-junction, which realizes a power continuous common flow connection as defined in (4), such that

$$f_S = \bar{f}_S, \quad \bar{e}_S = -e_S.$$

It is readily verified that Fig. 4 implements (6).

The submatrix $A(q,r)$ defines the relation between the rate of change of the state s of the elastic elements and the rate of change of the configuration of the internal DOFs q. Similarly, the submatrix $B(q,r)$ defines the relation between the rate of change of the state s of the springs and the rate of change of the output position r. Hence, the exact structure of $A(q,r)$ and $B(q,r)$ can be derived from a kinematic analysis of the actuator design.

B. Kinematic Structure of Variable Stiffness Actuators

It is assumed that the state s of the internal elastic elements is determined by the configuration q of the internal DOFs and the output position r via the kinematic relation

$$\begin{array}{rccc} \lambda: & \mathcal{Q}\times\mathcal{R} & \rightarrow & \mathcal{S} \\ & (q,r) & \mapsto & s. \end{array} \tag{7}$$

Note that the variables q and r are independent of each other, and their configuration determines the state of the internal elastic elements.

The tangent map, i.e., $\lambda_*: T_q\mathcal{Q}\times T_r\mathcal{R} \rightarrow T_s\mathcal{S}$, and the cotangent map, i.e., $\lambda^*: T_s^*\mathcal{S} \rightarrow T_q^*\mathcal{Q}\times T_r^*\mathcal{R}$, are naturally defined [18], where $T_q\mathcal{Q}$ ($T_q^*\mathcal{Q}$), $T_r\mathcal{R}$ ($T_r^*\mathcal{R}$), and $T_s\mathcal{S}$ ($T_s^*\mathcal{S}$) are the tangent (cotangent) spaces to the manifolds $\mathcal{Q}$, $\mathcal{R}$, and $\mathcal{S}$ at q, r, and s, respectively.

The tangent maps can be expressed in the natural coordinates on the tangent space as

$$\lambda_* = \left(\frac{\partial\lambda}{\partial q}(q,r), \frac{\partial\lambda}{\partial r}(q,r)\right) =: \left(A(q,r), B(q,r)\right).$$

Dually, the cotangent map can be expressed in the natural coordinates as

$$\lambda^* = \left(\frac{\partial^T\lambda}{\partial q^T}(q,r), \frac{\partial^T\lambda}{\partial r^T}(q,r)\right) =: \left(A^T(q,r), B^T(q,r)\right)$$

which completes the mathematical representation of the Dirac structure (6).

As observed already from (6), the tangent maps define the rate of change of the state s of the elastic elements as a result of the flows f_C and f_I. In particular, considering the natural coordinates on the tangent spaces, we have

$$\dot{s} = A(q,r)\dot{q} + B(q,r)\dot{r}. \tag{8}$$

In Fig. 5, the tangent map λ_* is visualized. More specifically, note that each of the maps, which are defined by $A(q,r)$ and $B(q,r)$, has an image space, which is a subspace of the tangent space $T_s\mathcal{S}$. The dimensions of the image of $A(q,r)$ depend on the number of internal elastic elements and the number of

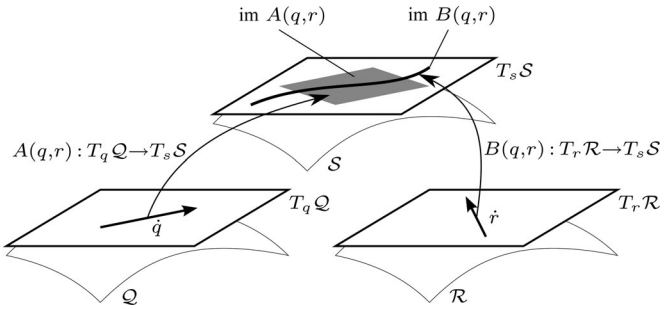

Fig. 5. Maps between the tangent spaces $T_q\mathcal{Q}$, $T_r\mathcal{R}$, and $T_s\mathcal{S}$. The image spaces of the maps $A(q,r)$ and $B(q,r)$ are subspaces of $T_s\mathcal{S}$.

internal DOFs, while the image of $B(q,r)$ is always one dimensional, since the actuator output is assumed to have only 1 DOF.

Under the map λ^*, it follows that $e_C = -A^T(q,r)e_S$ and $e_I = -B^T(q,r)e_S$, which state that the efforts τ and F depend on the effort e_S that is generated by the elastic elements. In particular, by the consideration of the natural coordinates on the cotangent space, the effort e_S is given by $\partial H/\partial s$, and through the map $A^T(q,r)$ and the map $B^T(q,r)$, respectively, we obtain

$$\tau = -A^T(q,r)\frac{\partial H}{\partial s} \quad \text{and} \quad F = -B^T(q,r)\frac{\partial H}{\partial s}.$$

We use this kinematic analysis to compute the power flows in variable stiffness actuators and, more specifically, in the various bonds of the model that is depicted in Fig. 4.

IV. Power-Flow Analysis

In this section, we provide a detailed study of the power flows in variable stiffness actuators using the port-based model that is presented in Section III. By the analysis of the kinematic structure of the actuators, we highlight the power transferred from the control port, i.e., the internal DOFs, to the internal elastic elements and to the output port. This analysis is facilitated by a change of coordinates on $T_s\mathcal{S}$ and $T_s^*\mathcal{S}$ that makes these power flows explicit. In particular, while the Dirac structure (6) describes the power distribution inside the variable stiffness actuator, it does not explicitly quantify the power exchange between the control and the output ports. A proper change of coordinates, as detailed in this section, allows the determination of how much control power can reach the output port. This is based on an analysis of the kinematics of the actuator and, more specifically, by examining the relation between the rate of change of the configuration variables of the actuation system, i.e., $\dot{s}$, $\dot{q}$, and $\dot{r}$, as defined by the maps between the tangent spaces that are described in Section III-B.

A. Change of Coordinates

The power flow between the internal elastic elements, the control, and the interaction ports is implicitly described in (3) and, in natural coordinates, is given by

$$\left\langle \frac{\partial H}{\partial s} \middle| \dot{s} \right\rangle = \left\langle \frac{\partial H}{\partial s} \middle| A(q,r)\dot{q} \right\rangle + \left\langle \frac{\partial H}{\partial s} \middle| B(q,r)\dot{r} \right\rangle$$

in which we assume that no dissipation is internally present. This means that the power flows are determined by the tangent maps $A(q,r)$ and $B(q,r)$. To further investigate the power flows, we define a new set of coordinates on $T_s\mathcal{S}$ and $T_s^*\mathcal{S}$ by using the image of the map $B(q,r)$.

Since the actuator output has only 1 DOF, i.e., r is 1-D, the image of the tangent map $B(q,r)$ is also 1-D, and in particular, it defines a line on $T_s\mathcal{S}$. Let $b^{\|}$ be a unit vector such that

$$\mathrm{im}B(q,r) = \mathrm{span}\{b^{\|}\}.$$

Then, a set of $n_s - 1$ unit vectors $b^{\perp}$ exists, such that

$$\mathrm{span}\{b^{\perp}\} = \mathrm{im}B^{\perp}(q,r).$$

The subspace $\mathrm{im}B^{\perp}(q,r)$ is the orthogonal complement to $\mathrm{im}B(q,r)$, and therefore, it is of dimension $n_s - 1$. This means that $\{b^{\|}, b^{\perp}\}$ forms a set of coordinate vectors that spans the tangent space $T_s\mathcal{S}$, i.e., $T_s\mathcal{S} = \mathrm{im}B(q,r) \oplus \mathrm{im}B^{\perp}(q,r)$.

Orthogonality on the tangent space $T_s\mathcal{S}$ is only defined if a proper metric is defined on it. Elements from $T_s\mathcal{S}$ represent the rate of change of the state s of the elastic elements, which may be, equivalently, considered as infinitesimal displacements δs. A physically meaningful metric to measure δs is the stiffness matrix [19], [20]. As stated in [21], in a conservative system, the stiffness matrix in configuration space coordinates is given by the Hessian of the potential energy function and can be shown to be a symmetric $(0,2)$-tensor and is, thus, a valid metric on $T_s\mathcal{S}$. In our case, if we consider the natural coordinates on $T_s\mathcal{S}$, the metric M is, therefore, given by

$$M = \frac{\partial^2 H}{\partial s^2}$$

where $H(s)$ describes the amount of elastic energy that is stored in the elastic elements. Note that the norm, i.e., $\|\delta s\|_M^2 = \delta s^T M \delta s$, which is induced by the metric M, has the unit of energy. If friction in the system is modeled, a different metric should be considered since the hypothesis of a conservative system is no longer valid.

As the metric M defines the inner product on $T_s\mathcal{S}$, the set $b^{\perp}$ is found by requiring

$$\langle b^{\|}, b_i^{\perp} \rangle_M = 0, \qquad i = 1, \ldots, n_s - 1$$

where $\langle \cdot, \cdot \rangle_M$ denotes the inner product with respect to the metric M.

We can now define a change of coordinates from the natural coordinates on $T_s\mathcal{S}$ to the new defined coordinates. Let S_b be a matrix that describe the change of coordinates as

$$S_b = [\, b^{\|} \quad b^{\perp} \,]. \tag{9}$$

Note that S_b depends on the state s of the elastic elements. If $\dot{s}$ is an element of $T_s\mathcal{S}$, which is expressed in the natural coordinates, and $\dot{s}^b$ is the same element, which is expressed in the coordinates $\{b^{\|}, b^{\perp}\}$, it follows that

$$\dot{s} = S_b \dot{s}^b \tag{10}$$

and since the change of coordinates is by construction invertible, it follows that $\dot{s}^b = S_b^{-1}\dot{s}$.

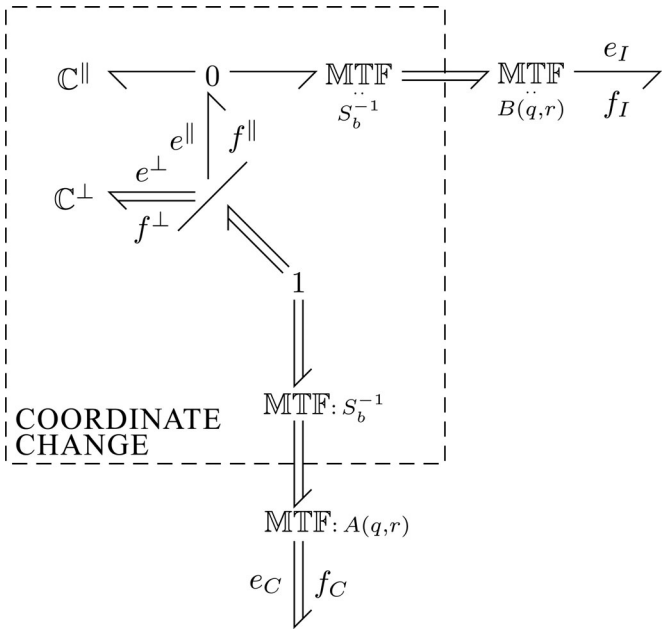

Fig. 6. Visualization of the virtual storage elements. The change of coordinates S_b^{-1} can be realized by two $\mathbb{MTF}$-elements and a power splitter (the diagonally oriented line). The two $\mathbb{C}$-elements, i.e., $\mathbb{C}^{\|}$ and $\mathbb{C}^{\perp}$, represent the virtual storage elements.

The elements on $T_s\mathcal{S}$ that are defined in (8) can be expressed in the new coordinates. In particular, we have

$$\begin{aligned}\dot{s}^b &= S_b^{-1}\dot{s}\\ &= S_b^{-1}\left(A(q,r)\dot{q} + B(q,r)\dot{r}\right)\\ &=: S_b^{-1}\left(\dot{s}_q + \dot{s}_r\right)\\ &=: \begin{pmatrix}\dot{s}_q^{\|}\\ \dot{s}_q^{\perp}\end{pmatrix} + \begin{pmatrix}\dot{s}_r^{\|}\\ \dot{s}_r^{\perp}\end{pmatrix} =: \begin{pmatrix}\dot{s}^{\|}\\ \dot{s}^{\perp}\end{pmatrix}. \end{aligned} \tag{11}$$

The element $\dot{s}_r^{\perp}$ is zero by construction of the coordinate set.

Essentially, with this change of coordinates, from the real elastic element $\mathbb{C}$ with state s, we create two virtual storage elements $\mathbb{C}^{\|}$ and $\mathbb{C}^{\perp}$, with states $s^{\|}$ and $s^{\perp}$, respectively. By construction, the state $s^{\|}$ is one dimensional, and the state $s^{\perp}$ has the dimension $n_s - 1$. This scenario is depicted in Fig. 6. From (11), it can be noted that the virtual storage element $\mathbb{C}^{\perp}$ is not connected to the output, i.e., it captures the energy that is supplied via the control port without redistributing it to the output.

B. Power Flows

Only when the change of coordinates (10) is also applied to elements of the cotangent space $T_s^*\mathcal{S}$, the power flows to $\mathbb{C}^{\|}$ and $\mathbb{C}^{\perp}$ can be analyzed. On $T_s^*\mathcal{S}$, the change of coordinates results in the transformation of efforts as [18]

$$\frac{\partial^T H}{\partial s^T} S_b =: \begin{pmatrix} F_S^{\|} & F_S^{\perp}\end{pmatrix}. \tag{12}$$

The port behavior of the two virtual storage elements $\mathbb{C}^{\|}$ and $\mathbb{C}^{\perp}$ can now be properly defined by using (11) and (12), i.e.,

$$\begin{aligned}\dot{s}^{\|} &= \dot{s}_q^{\|} + \dot{s}_r^{\|}, \quad e_S^{\|} = F_S^{\|}\\ \dot{s}^{\perp} &= \dot{s}_q^{\perp}, \quad e_S^{\perp} = F_S^{\perp}.\end{aligned}$$

The power supplied via the control port is given by

$$P_C = \langle e_C | f_C \rangle = -\langle A^T(q,r)\, e_S | \dot{q}\rangle = -\left\langle \frac{\partial H}{\partial s}\middle| \dot{s}_q \right\rangle$$

and expressions for the power flows from the control port toward the two virtual storage elements are

$$P_C^{\|} = -\langle F_S^{\|} | \dot{s}_q^{\|}\rangle \tag{13}$$

$$P_C^{\perp} = -\langle F_S^{\perp} | \dot{s}_q^{\perp}\rangle. \tag{14}$$

It is readily verified that the change of coordinates is power continuous, i.e.,

$$P_C^{\|} + P_C^{\perp} = P_C.$$

Remark 1: Note that the dynamical behavior of the load is not modeled, and therefore, the proposed analysis is task independent. The power flow P_L to the load is given by $P_L = P_C - P^{\|} - P^{\perp}$, in which $P^{\|}$ cannot be computed. However, since there is a direct connection between $\mathbb{C}^{\|}$ and the output, by means of the 0-junction, the power flow $P^{\|}$ can be used to do work on the output. On the other hand, the power flow $P^{\perp}$ is completely captured by $\mathbb{C}^{\perp}$. It represents the power that is supplied by the control port, which cannot be used to do any work on the output, but is instead internally stored in the actuator because of its kinematic structure.

Remark 2: The image of the map $B(q,r)$ defines an involutive distribution on $\mathcal{S}$ with dimension 1, since the output has only 1 DOF. If the set $\{b^{\perp}\}$ is not empty, then, for any configuration (q,r), there exists a foliation $\mathcal{S}_r$ that is the integral manifold of this distribution [18]. This integral manifold is also 1-D. Since the energy function $H(s)$ is positive semidefinite by definition, it has a minimum on $\mathcal{S}_r$, which defines how much energy can go out from the elastic elements via the output port. However, this minimum is, in general, not the same as the global minimum of $H(s)$ on $\mathcal{S}$. Hence, there is energy stored in the elastic elements that cannot be used to do work on the output.

C. Power-Flow Ratio

The change of coordinates and the subsequent definition of power flows in (13) and (14), as visualized in Fig. 6, give rise to the definition of a power-flow ratio. As already observed, the virtual power flow $P_C^{\perp}$ is disconnected from the output, and thus, it cannot be used to do work at the output. Intuitively, the ratio

$$\mu = \frac{P_C^{\perp}}{P_C} \tag{15}$$

indicates how much of the power that is supplied via the control port is, in fact, captured by the virtual storage element $\mathbb{C}^{\perp}$ and, therefore, lost: The lower this measure is, the less the energy is captured by the elastic elements. Note that $\mu \in [0,1]$.

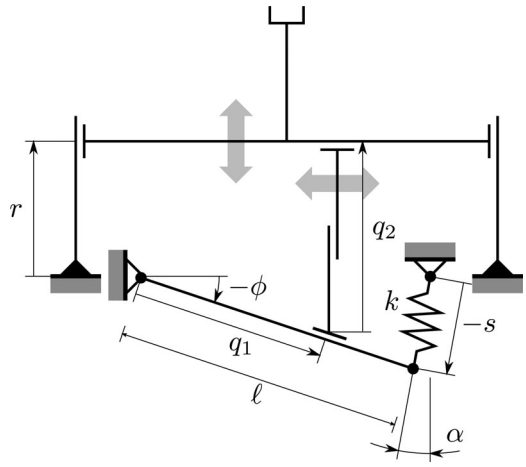

Fig. 7. Variable stiffness actuator using a lever arm of variable length. The functional principle of the concept is a lever arm of variable length q_1, which connects the zero-free-length linear spring, with elastic constant k, to the output. The effective length of the lever arm is determined by the linear DOF q_1. The actuator output position r is controlled by the linear DOF q_2 [10], [11].

Since the coordinate change is configuration dependent, the power-flow ratio μ is a dynamic measure of power flows. The rationale in this analysis is that instantaneous power that is provided by the controller should provide an instantaneous power flow to the output and should closely match the provided power flow from the controller.

V. Analysis of Conceptual Variable Stiffness Actuator Designs

In this section, we analyze the working principles of three designs of variable stiffness actuators, which realize a variable output stiffness by means of different kinematic structures. As follows from the previous sections, the power flows to the virtual storage elements are defined by the maps $A(q,r)$ and $B(q,r)$, i.e., by the kinematic properties of the actuator design. First, we present the model of the designs in a port-based formalism, and then, we proceed by the evaluation of the power-flow ratio μ, as defined in (15).

A. Design Based on a Lever Arm of Variable Length

In some designs, such as vsaUT [10], [11], AwAS [12], AwAS-II [13], and HDAU [14], the change of the output stiffness is realized through a change of the transmission ratio between the internal springs and the actuator output by means of a lever arm of variable length.

As an example of this category of variable stiffness actuators, we analyze the vsaUT, which is conceptually depicted in Fig. 7. The working principle is based on one zero-free-length linear spring, which is characterized by the elastic constant k. The spring is connected to the output via a lever arm of variable length, which is controlled by the linear DOF q_1, and thus, q_1 determines how the spring is sensed at the output. The linear DOF q_2 is used to control the actuator output position, i.e., the configuration variable r. The design is such that the maximum length ℓ of the lever arm is sufficiently large compared with the maximum elongation of the spring so that we can assume $\alpha \approx 0$.

In order to build the port-based model of this actuator design, we analyze its kinematics, which are described in (7). We observe that the state s of the zero-free-length linear spring is given by

$$s = \ell \sin\phi = \ell \frac{r - q_2}{q_1}. \tag{16}$$

By taking the total derivative of the aforementioned equation, it follows that

$$\dot{s} = -\frac{\ell}{q_1}\begin{bmatrix} \frac{r-q_2}{q_1} & 1 \end{bmatrix}\begin{bmatrix} \dot{q}_1 \\ \dot{q}_2 \end{bmatrix} + \frac{\ell}{q_1}\dot{r} =: f_S.$$

From this equation, we can identify the matrices $A(q,r)$ and $B(q,r)$ as

$$A(q,r) = -\frac{\ell}{q_1}\begin{bmatrix} \frac{r-q_2}{q_1} & 1 \end{bmatrix} \quad \text{and} \quad B(q) = \frac{\ell}{q_1}$$

with which it is possible to build the skew-symmetric matrix $D(q,r)$ that represents the Dirac structure, as defined in (6).

Since only one spring is present, the tangent space $T_s\mathcal{S}$ is one dimensional. The image of $B(q,r)$ is given by

$$\mathrm{im}B(q,r) = T_s\mathcal{S} \qquad \forall (q,r) \in \mathcal{Q} \times \mathcal{R}.$$

It follows that the virtual storage element $\mathbb{C}^{\perp}$ has 0-D, i.e., it does not appear in the diagram of Fig. 6. Therefore, all the power P_C, which is supplied via the control port during any nominal behavior of the actuator, goes either to $\mathbb{C}^{\parallel}$ or to the output. This means that no power is lost, i.e., no energy is captured by the internal springs. This means that, for this principle design, the power-flow ratio μ, as defined in (15), is

$$\mu = 0.$$

This observation is in accordance with the static analysis that is presented in [15], where it was shown that the designs that are based on a variable length lever arm do not require any storage of energy in the internal springs when the apparent output stiffness is changed.

B. Design Based on an Antagonistic Spring Setup

Variable stiffness actuators, which are based on an antagonistic spring setup, have been proposed in different realizations, such as the AMASC [22], VSA [7], and VSA-II [8]. In general, the designs use nonlinear springs that act in opposite directions on the output. The internal DOFs change the elongation of the springs, and this way, they indirectly change the actuator output position and the apparent output stiffness.

The conceptual design of a generic antagonistic variable stiffness actuator is depicted in Fig. 8. The working principle is based on two identical nonlinear quadratic springs, which are characterized by the elastic constant k. The springs are in series with two linear motors M_1 and M_2, which generate the two linear displacements q_1 and q_2, respectively. When the motors are operated in the common mode, the actuator output stiffness is changed. When the motors are operated in the differential mode, the actuator output position r is changed.

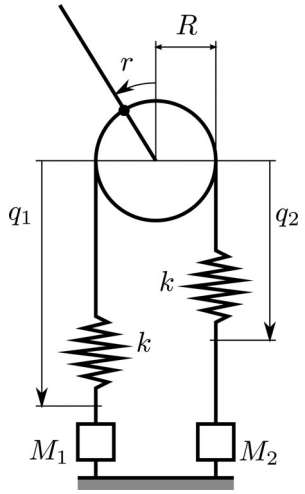

Fig. 8. Variable stiffness actuator using an antagonistic spring setup. This design is based on two series elastic actuators in an antagonistic setup. The linear motors M_1 and M_2 generate, respectively, the linear displacements q_1 and q_2. The nonlinear quadratic springs have the elastic constant k. By operating the motors in the common mode, the apparent output stiffness of the actuator changes, while by operating the motors in the differential mode, the equilibrium of the actuator output position r changes.

In order to build the port-based model of this actuator design, we analyze its kinematics, which are described in (7). We observe that the states $s_i > 0$, with $i = 1, 2$, of the nonlinear springs are given by

$$s = \begin{bmatrix} s_1 \\ s_2 \end{bmatrix} = \begin{bmatrix} q_1 - Rr \\ q_2 + Rr \end{bmatrix} \tag{17}$$

where R is the radius of the pulley, and the restriction $s_i > 0$ is assumed to simplify the equations involving the force generated by the quadratic springs. By taking the total derivative of (17), we obtain

$$\dot{s} = \begin{bmatrix} \dot{s}_1 \\ \dot{s}_2 \end{bmatrix} = \begin{bmatrix} \dot{q}_1 - R\dot{r} \\ \dot{q}_2 + R\dot{r} \end{bmatrix} =: \begin{bmatrix} f_{S_1} \\ f_{S_2} \end{bmatrix}.$$

From this, we can identify the matrices $A(q, r)$ and $B(q, r)$ as

$$A(q, r) = \begin{bmatrix} 1 & 0 \\ 0 & 1 \end{bmatrix} \quad \text{and} \quad B(q, r) = \begin{bmatrix} -R \\ R \end{bmatrix}$$

with which it is possible to build the skew-symmetric matrix $D(q, r)$ that represents the Dirac structure, as defined in (6).

As this design presents two springs, the tangent space $T_s\mathcal{S}$ is two dimensional. Let the metric M be

$$M = \frac{\partial^2 H}{\partial s^2} = \begin{bmatrix} 2ks_1 & 0 \\ 0 & 2ks_2 \end{bmatrix}$$

where $H(s) = (1/3)ks_1^2 + (1/3)ks_2^2$ is the elastic energy of the nonlinear quadratic springs. The unit vector $b^{\|}$, which is computed with respect to the metric M, such that $\|b^{\|}\|_M = 1$, is

$$b^{\|} = \frac{1}{\sqrt{2k(s_1 + s_2)}} \begin{bmatrix} -1 \\ 1 \end{bmatrix}.$$

By the use of the constraints on the orthogonality, i.e., $\langle b^{\|}, b^{\perp} \rangle_M = 0$, the unit vector $b^{\perp}$, which is computed with respect to the metric M, such that $\|b^{\perp}\|_M = 1$, is

$$b^{\perp} = \frac{1}{\sqrt{2k(s_1 + s_2)}} \begin{bmatrix} \sqrt{\frac{s_2}{s_1}} \\ \sqrt{\frac{s_1}{s_2}} \end{bmatrix}.$$

The change of coordinates, as defined in (9), follows

$$S_b = [\, b^{\|} \quad b^{\perp} \,] = \frac{1}{\sqrt{2k(s_1 + s_2)}} \begin{bmatrix} -1 & \sqrt{\frac{s_2}{s_1}} \\ 1 & \sqrt{\frac{s_1}{s_2}} \end{bmatrix}.$$

In order to continue the power analysis that is presented in Section IV, we calculate

$$\begin{aligned} \begin{pmatrix} \dot{s}_q^{\|} \\ \dot{s}_q^{\perp} \end{pmatrix} &= S_b^{-1} A(q, r) \dot{q} \\ &= \frac{\sqrt{2k(s_1 + s_2)}}{s_1 + s_2} \begin{bmatrix} -s_1 & s_2 \\ \sqrt{s_1 s_2} & \sqrt{s_1 s_2} \end{bmatrix} \begin{bmatrix} 1 & 0 \\ 0 & 1 \end{bmatrix} \begin{bmatrix} \dot{q}_1 \\ \dot{q}_2 \end{bmatrix} \\ &= \frac{\sqrt{2k(s_1 + s_2)}}{s_1 + s_2} \begin{bmatrix} -s_1 \dot{q}_1 + s_2 \dot{q}_2 \\ \sqrt{s_1 s_2}(\dot{q}_1 + \dot{q}_2) \end{bmatrix}. \end{aligned}$$

The quadratic springs generate forces, i.e., $e_S = \partial H / \partial s = [\, ks_1^2 \quad ks_2^2 \,]^T$, from which we obtain

$$\begin{aligned} \begin{pmatrix} F_S^{\|} & F_S^{\perp} \end{pmatrix} &= \frac{\partial^T H}{\partial s^T} S_b \\ &= [\, ks_1^2 \quad ks_2^2 \,] \frac{1}{\sqrt{2k(s_1 + s_2)}} \begin{bmatrix} -1 & \sqrt{\frac{s_2}{s_1}} \\ 1 & \sqrt{\frac{s_1}{s_2}} \end{bmatrix} \\ &= \frac{1}{\sqrt{2k(s_1 + s_2)}} \begin{bmatrix} k\big(-s_1^2 + s_2^2\big) & k\big(\sqrt{s_1^3 s_2} + \sqrt{s_1 s_2^3}\big) \end{bmatrix}. \end{aligned} \tag{18}$$

The power-flow ratio μ, as defined in (15), is given by

$$\mu = \frac{P_C^{\perp}}{P_C} = \frac{\langle F_S^{\perp} | \dot{s}_q^{\perp} \rangle}{\langle \frac{\partial H}{\partial s} | \dot{s}_q \rangle}.$$

Since μ is a dynamic measure, we can compute it during any nominal behavior of the variable stiffness actuator. The power-flow ratio is visualized in Fig. 9, where $\dot{q}$ has been chosen to achieve certain desired changes in the output position $\dot{r}$ and stiffness $\dot{K}$. The areas indicate that, for a particular $(\dot{r}, \dot{K})$, the value of μ is in the corresponding area. For example, the power-flow ratio μ is in the area that is denoted by μ_1 when the output stiffness is changed with $\dot{K} = 0.2$ N·m/rad/s and when the output position r is changed simultaneously. The actual value of μ depends on the load of the springs, i.e., (s_1, s_2), and it is negatively affected by higher preloads, which is in agreement with [15]. From (18), it can be seen that $P^{\|} = \langle F_S^{\|} | \dot{s}_q^{\|} \rangle = 0$, if $s_1 = s_2$, and hence, because of power continuity, $\mu = 1$. Finally, note

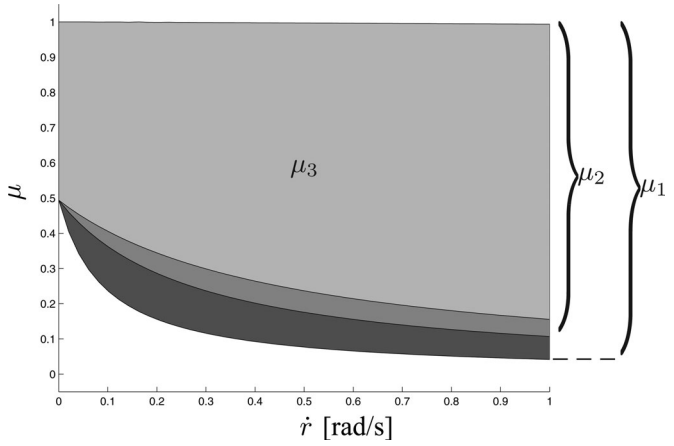

Fig. 9. Power-flow ratio μ for the design based on an antagonistic spring setup. The rate of change of the configuration variable $\dot{q}$ of the internal DOFs is chosen to achieve the desired changes in the output position $\dot{r}$ and stiffness $\dot{K}$. The indicated areas μ_1, μ_2, and μ_3 correspond to $\dot{K} = 0.2$ N·m/rad/s, $\dot{K} = 0.6$ N·m/rad/s, and $\dot{K} = 1$ N·m/rad/s, respectively.

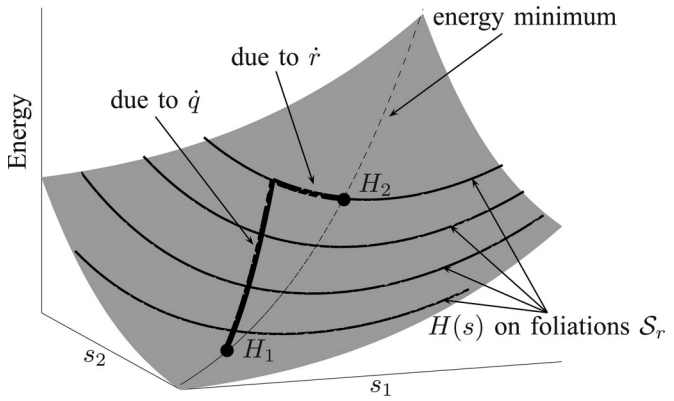

Fig. 10. Energy function on $\mathcal{S}$. The surface represents the energy function $H(s)$ on $\mathcal{S}$. Since the image of $A(q,r)$ spans the entire tangent space $T_s\mathcal{S}$, any arbitrary point $s \in \mathcal{S}$ can be reached by a proper $\dot{q}$. However, restricted to the foliations $\mathcal{S}_r$ (indicated by the black lines), only a local minimum of $H(s)$ can be reached (indicated by the dashed line). The difference in energy levels between the end points of the thick black curve, i.e., $H_2 - H_1$, indicates how much energy cannot be used to do work on the output.

that the power-flow ratio increases when the stiffness change is faster.

For this particular design principle, Remark 2 can be illustrated visually. In Fig. 10, the surface represents the energy function, i.e., $H(s) = \frac{1}{3}ks_1^3 + \frac{1}{3}ks_2^3$, on the manifold $\mathcal{S}$, and the black curves represent the energy function on the integral manifolds $\mathcal{S}_r$ of $B(q,r)\dot{r}$. Restricted to these foliations, $H(s)$ has a minimum that is indicated by the dashed line. Since the matrix $A(q,r)$ is full rank for this design, the integral manifold of $A(q,r)\dot{q}$ is in fact equal to $\mathcal{S}$. This means that, by the use of the control input $\dot{q}$ with its corresponding control energy, it is possible to go from any configuration on $\mathcal{S}$ to any other configuration. However, through the output port, the configuration change is restricted to lie on the foliation $\mathcal{S}_r$ that has been reached. Therefore, the minimum energy level that the system can reach is in a local minimum of $H(s)$. This is illustrated

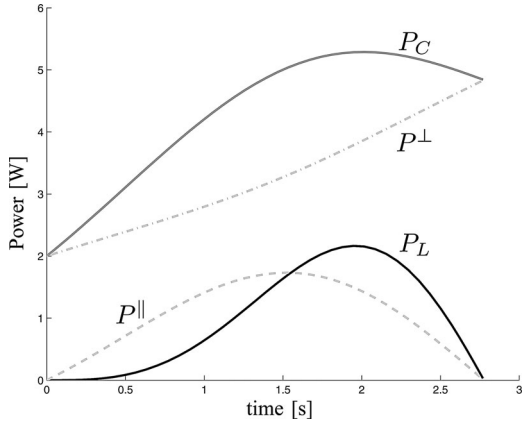

Fig. 11. Power flow. The power supplied via the control port is used to accelerate the mass. Initially, all the power is stored in $\mathbb{C}^\parallel$ and $\mathbb{C}^\perp$, i.e., $P_L = 0$, because of the inertia of the load. When $P^\parallel > P_L$, power is flowing toward $\mathbb{C}^\parallel$ and stored, but later, when $P^\parallel < P_L$, power is flowing from $C^\parallel$ to the load.

via the solid black curve, which represents a generic change of configuration of the actuator. It can be seen that, in general, the energy, which has been supplied via the control port, cannot be provided completely to the output port. The actual amount of energy that is internally stored is equal to the difference in energy levels at the end points of the solid curve, i.e., $H_2 - H_1$.

Example: The simple structure of this type of actuator allows to illustrate the theory with a straightforward simulation experiment. We assume that a mass is attached to the output and that, starting from a zero velocity, it should achieve a constant $\dot{r}$, while the apparent output stiffness is changed, simultaneously, with constant $\dot{K}$. It follows that the control input $\dot{q}$ is also constant.

Fig. 11 presents the power flow $P^\parallel$ to the virtual storage element $\mathbb{C}^\parallel$, the power flow $P^\perp$ to the virtual storage element $\mathbb{C}^\perp$, the total power flow P_C from the control port, and the power flow P_L to the load.

Initially, all power is stored as potential energy in $\mathbb{C}^\parallel$ and $\mathbb{C}^\perp$, because of the inertia of the load, and therefore, the power flows $P^\parallel$ and $P^\perp$ increase. While $P^\parallel > P_L$, the mass accelerates and the power P_C is diverted to $\mathbb{C}^\parallel$ and stored as potential energy. When $P^\parallel \leq P_L$, this potential energy is started to be released to the load. Note that $P^\perp$ is always increasing, which means that part of the control power P_C is captured by the internal springs and not used to accelerate the mass.

Fig. 12 presents the energy balance between the energy H_C that is supplied by the controller and the kinetic energy H_L of the load. Because, throughout the experiment, $P_C > P^\parallel$, the controller supplies much more energy than is converted to the kinetic energy of the load. In fact, the difference, $H_C - H_L$, is stored internally in the springs.

C. Design Based on a Mechanical Decoupling

In other designs, such as the VS-Joint [9], the change of the apparent output stiffness and the change of the output joint position is completely mechanically decoupled. The conceptual design of this kind of actuators is depicted in Fig. 13. The working principle is based on two identical nonlinear quadratic

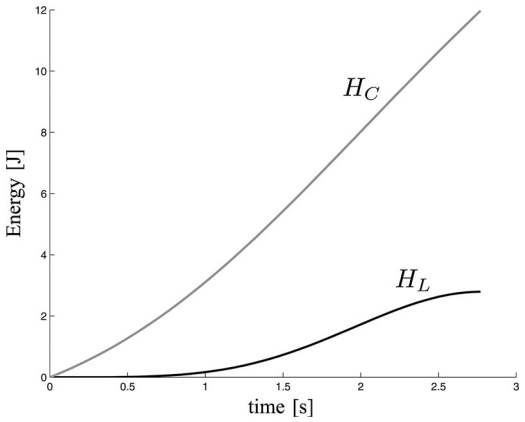

Fig. 12. Energy balance. During the acceleration of the mass, the energy that is supplied by the controller is bigger than the energy that is converted to the kinetic energy of the load.

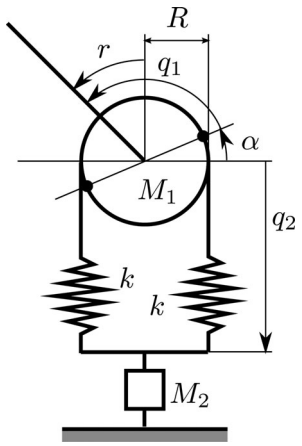

Fig. 13. Variable stiffness actuator using an antagonistic spring configuration and based on mechanical decoupling. In this design, the change of the stiffness and the actuator output position r is decoupled. The linear motor M_2 generates a linear displacement q_2 and is used to change the apparent output stiffness of the actuator. The output joint position r is determined by the rotational motor M_1.

springs, which are characterized by the elastic constant k. The linear motor M_2 generates a linear displacement q_2 and is used to change the apparent output stiffness of the actuator. The output position r is determined by the rotational motor M_1, which directly controls the DOF q_1. Note that, thus, the end effector can rotate independently of the pulley. Compared with the antagonistic design that is presented in Section V-B, the DOF q_1 realizes the differential mode of the operation of the motors M_1 and M_2 in the antagonistic design, and the DOF q_2 realizes the common-mode operation.

In order to build the port-based model of this actuator design, we analyze its kinematics, which is described in (7). We observe that the states $s_i > 0$, with $i = 1, 2$, of the nonlinear spring are given by

$$s = \begin{bmatrix} s_1 \\ s_2 \end{bmatrix} = \begin{bmatrix} q_2 - R\alpha \\ q_2 + R\alpha \end{bmatrix} \tag{19}$$

where R is the radius of the pulley; $\alpha = -q_1 + r + \pi/2$; and the restriction $s_i > 0$ is assumed to simplify the equations that involve the force generated by the quadratic springs. By taking

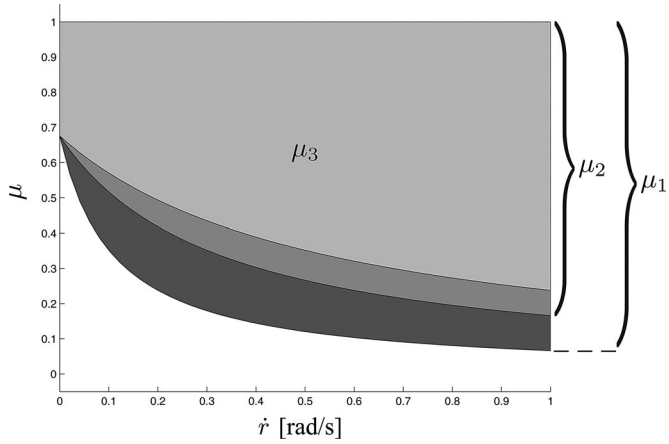

Fig. 14. Power-flow ratio μ for the design based on mechanical decoupling. The rate of change of the configuration variable $\dot{q}$ of the internal DOFs is chosen to achieve the desired changes in the output position $\dot{r}$ and stiffness $\dot{K}$. The indicated areas μ_1, μ_2, and μ_3 correspond to $\dot{K} = 0.2$ N·m/rad/s, $\dot{K} = 0.6$ N·m/rad/s, and $\dot{K} = 1.0$ N·m/rad/s, respectively.

the total derivative of (19), we obtain

$$\dot{s} = \begin{bmatrix} \dot{s}_1 \\ \dot{s}_2 \end{bmatrix} = \begin{bmatrix} \dot{q}_2 + R\dot{q}_1 - R\dot{r} \\ \dot{q}_2 - R\dot{q}_1 + R\dot{r} \end{bmatrix} =: \begin{bmatrix} f_{S_1} \\ f_{S_2} \end{bmatrix}.$$

From this, we identify the matrices $A(q, r)$ and $B(q, r)$, as

$$A(q,r) = \begin{bmatrix} R & 1 \\ -R & 1 \end{bmatrix} \quad \text{and} \quad B(q,r) = \begin{bmatrix} -R \\ R \end{bmatrix}$$

with which the Dirac structure, as defined in (6), can be represented.

The matrix $B(q, r)$ for this design is the same as for the previous design. Hence, the image is exactly the same, and the same change of coordinates S_b is obtained. We then have

$$\begin{aligned} \begin{pmatrix} \dot{s}_q^{\parallel} \\ \dot{s}_q^{\perp} \end{pmatrix} &= S_b^{-1} A(q,r)\dot{q} \\ &= \frac{\sqrt{2k(s_1+s_2)}}{s_1+s_2} \begin{bmatrix} -s_1 & s_2 \\ \sqrt{s_1 s_2} & \sqrt{s_1 s_2} \end{bmatrix} \begin{bmatrix} R & 1 \\ -R & 1 \end{bmatrix} \begin{bmatrix} \dot{q}_1 \\ \dot{q}_2 \end{bmatrix} \\ &= \frac{\sqrt{2k(s_1+s_2)}}{s_1+s_2} \begin{bmatrix} -R\dot{q}_1(s_1+s_2) - \dot{q}_2(s_1-s_2) \\ 2\sqrt{s_1 s_2}\dot{q}_2 \end{bmatrix}. \end{aligned}$$

The forces, i.e., $e_S = \partial H/\partial s$, are the same as in the antagonistic design, and hence, we can compute μ according to (15)

$$\mu = \frac{P_C^{\perp}}{P_C} = \frac{\langle F_S^{\perp} | \dot{s}_q^{\perp} \rangle}{\langle \frac{\partial H}{\partial s} | \dot{s}_q \rangle}.$$

Fig. 14 presents a visualization of the power-flow ratio, where $\dot{q}_1$ has been used to achieve the indicated $\dot{r}$, and $\dot{q}_2$ to achieve $\dot{K}$. The areas indicate that, for a particular $(\dot{r}, \dot{K})$, the value of μ will be in the corresponding area. In addition, for this design, the actual value of μ depends on the load of the springs, i.e., (s_1, s_2), and it is negatively affected by higher preloads. As in the previous design, it can be noted that the power-flow ratio increases when the stiffness change is faster. However, because of the mechanical decoupling of the position and stiffness change, this influence is bigger than in the previous design.

VI. Conclusion

In this paper, a power-flow ratio for variable stiffness actuators has been defined, which is derived by using a port-based modeling framework. The power-flow ratio has been computed under dynamic conditions, and it has been determined how the working principle of the actuator allows in transferring the power from the internal DOFs to the output, irrespective of the dynamic behavior of the load. We have shown in three different principle designs that the power-flow ratio is strictly related to the kinematic properties of the actuator, i.e., to its topological structure.

It has been observed that the pretension of the internal elastic elements has a negative influence on the power-flow ratio. This can be explained by the observation of the relation between the output motion and the state of the internal springs. We have shown that this effect becomes more prominent when the rate of change of the stiffness increases.

From the power-flow analysis, it can be concluded that for variable stiffness actuators, which are realized by a variable transmission ratio between the output and the internal springs, all the power that is supplied by the control port can be used to do work on the output without being captured by the internal elastic elements. Therefore, this working principle allows a more efficient distribution of the power flow from the control port.

The power-flow analysis and the definition of the power-flow ratio, as presented in this study, give important insights into the design of variable stiffness actuator and the design of control laws.

References

[1] N. Hogan, "Impedance control: An approach to manipulation: Part I–Theory," *J. Dyn. Syst., Meas., Control*, vol. 107, no. 1, pp. 1–7, 1985.

[2] A. Bicchi and G. Tonietti, "Fast and 'soft-arm' tactics: Dealing with the safety-performance tradeoff in robot arms design and control," *IEEE Robot. Autom. Mag.*, vol. 11, no. 2, pp. 22–33, Jun. 2004.

[3] A. Albu-Schäffer, O. Eiberger, M. Grebenstein, S. Haddadin, C. Ott, T. Wimböck, S. Wolf, and G. Hirzinger, "Soft robotics," *IEEE Robot. Autom. Mag.*, vol. 15, no. 3, pp. 20–30, Sep. 2008.

[4] R. van Ham, T. Sugar, B. Vanderborght, K. Hollander, and D. Lefeber, "Compliant actuator designs," *IEEE Robot. Autom. Mag.*, vol. 16, no. 3, pp. 81–94, Sep. 2009.

[5] K. Hollander, T. Sugar, and D. Herring, "Adjustable robotics tendon using a 'Jack Spring'™," in *Proc. Int. Conf. Rehabil. Robot.*, 2005, pp. 113–118.

[6] J. Choi, S. Park, W. Lee, and S.-C. Kang, "Design of a robot joint with variable stiffness," in *Proc. IEEE Int. Conf. Robot. Autom.*, 2008, pp. 1760–1765.

[7] G. Tonietti, R. Schiavi, and A. Bicchi, "Design and control of a variable stiffness actuator for safe and fast physical human/robot interaction," in *Proc. IEEE Int. Conf. Robot. Autom.*, 2005, pp. 526–531.

[8] R. Schiavi, G. Grioli, S. Sen, and A. Bicchi, "VSA-II: A novel prototype of variable stiffness actuator for safe and performing robots interacting with humans," in *Proc. IEEE Int. Conf. Robot. Autom.*, 2008, pp. 2171–2176.

[9] S. Wolf and G. Hirzinger, "A new variable stiffness design: Matching requirements of the next robot generation," in *Proc. IEEE Int. Conf. Robot. Autom.*, 2008, pp. 1741–1746.

[10] L. C. Visser, R. Carloni, R. Ünal, and S. Stramigioli, "Modeling and design of energy efficient variable stiffness actuators," in *Proc. IEEE Int. Conf. Robot. Autom.*, 2010, pp. 3273–3278.

[11] L. C. Visser, R. Carloni, and S. Stramigioli, "Energy efficient variable stiffness actuators," *IEEE Trans. Robot.*, vol. 27, no. 5, pp. 1–11, Jun. 2011.

[12] A. Jafari, N. Tsagarakis, B. Vanderborght, and D. Caldwell, "A novel actuator with adjustable stiffness (AwAS)," in *Proc. IEEE/RSJ Int. Conf. Intell. Robots Syst.*, 2010, pp. 4201–4206.

[13] A. Jafari, N. Tsagarakis, B. Vanderborght, and D. Caldwell, "AwAS-II: A new actuator with adjustable stiffness based on the novel principle of adaptable pivot point and variable lever ratio," in *Proc. IEEE Int. Conf. Robot. Autom.*, 2011, pp. 4638–4643.

[14] B.-S. Kim and J.-B. Song, "Hybrid dual actuator unit: A design of a variable stiffness actuator based on an adjustable moment arm mechanism," in *Proc. IEEE Int. Conf. Robot. Autom.*, 2010, pp. 1655–1660.

[15] L. C. Visser, R. Carloni, and S. Stramigioli, "Variable stiffness actuators: A port-based analysis and a comparison of energy efficiency," in *Proc. IEEE Int. Conf. Robot. Autom.*, 2010, pp. 3279–3284.

[16] V. Duindam, A. Macchelli, S. Stramigioli, and H. Bruyninckx, *Modeling and Control of Complex Physical Systems*. New York: Springer-Verlag, 2009.

[17] S. Stramigioli, *Modeling and IPC Control of Interactive Mechanical Systems: A Coordinate-free Approach*. New York: Springer-Verlag, 2001.

[18] H. Nijmeijer and A. van der Schaft, *Nonlinear Dynamical Control Systems*. New York: Springer-Verlag, 1990.

[19] M. W. Griffis, "Kinestatic control: A novel theory for simultaneously regulating force and displacement," Ph.D. dissertation, Dept. Mech. Eng., Univ. Florida, Gainesville, 1991.

[20] M. Griffis and J. Duffy, "Global stiffness modeling of a class of simple compliant couplings," *Mech. Mach. Theory*, vol. 28, no. 2, pp. 207–224, 1993.

[21] M. Zefran and V. Kumar, "Affine connections for the cartesian stiffness matrix," in *Proc. IEEE Int. Conf. Robot. Autom.*, 1997, pp. 1376–1381.

[22] J. Hurst, J. Chestnutt, and A. Rizzi, "An actuator with physically variable stiffness for highly dynamic legged locomotion," in *Proc. IEEE Int. Conf. Robot. Autom.*, 2004, pp. 4662–4667.

Raffaella Carloni (M'08) received the M.Sc. and Ph.D. degrees from the University of Bologna, Bologna, Italy.

She is an Assistant Professor with the Control Engineering Group, University of Twente, Enschede, The Netherlands, within the Center of Excellence on Intelligent Mechatronic Systems. Her research interests include robotic manipulation, control of complex dynamical systems, novel actuators for locomotion, and prosthetic devices.

Dr. Carloni has been an Associate Editor for the IEEE Robotics and Automation Magazine since 2010.

Ludo C. Visser (S'08) received the M.Sc. degree in electrical engineering, with main focus on control and robotics, from the University of Twente, Enschede, The Netherlands, in 2008. He is currently working toward the Ph.D. degree with the Control Engineering Group, University of Twente, under the supervision of Prof. S. Stramigioli and Dr. R. Carloni. During his research, he visited the Università di Pisa, Pisa, Italy, to work with Prof. A. Bicchi.

He was a Visiting Student with Oakland University, Rochester, MI. His research interests include modeling, design, and control of variable stiffness actuators.

Stefano Stramigioli (SM'03) received the M.Sc. degree from the University of Bologna, Bologna, Italy, and the Ph.D. degree from Delft University of Technology, Delft, The Netherlands, in 1992 and 1998, respectively.

He was a Researcher with the University of Twente, Enschede, The Netherlands, while working toward the M.Sc. and Ph.D. degrees. He is currently a Full Professor of advanced robotics and the Chair Holder of the Control Engineering group with the University of Twente. He has authored/coauthored more than 150 publications, including four books, book chapters, and journal and conference contributions.

Prof. Stramigioli is the Emeritus Editor-in-Chief of the IEEE Robotics and Automation Magazine, which is the journal in the field of robotics with the highest impact factor 3. He is also the Editor-in-Chief of the IEEE Intelligent Transportation Systems Council Newsletter. He is a member of the Editorial Board of the *Springer Journal of Intelligent Service Robotics*, and he is currently the Vice President for Member Activities of the IEEE Robotics and Automation Society (RAS). He is an AdCom Member of the IEEE RAS.